Differential Tomography: Influence of Sensitivity Direction and Noise-suppressing Windows

Sebastian Kaeppler, Andreas Maier, Christian Riess

***Abstract*—Phase-sensitive systems can deliver improved CT imaging performance for materials with low attenuation contrast, and, due to the differential nature of their images, when high spatial resolution is required. Typically, these systems only yield a directional derivative of a projection image along one sensitivity direction. The sensitivity direction is usually tangential to the CT trajectory. However, it is also conceivable to build systems with other sensitivity directions.**

The purpose of this paper is two-fold. First, we investigate the noise behavior of differential CT for sensitivity directions in z-direction and for bi-directional projections. Second, we use Wiener filtering to derive noise-suppressing window functions for all three sensitivity directions.

Our experiments indicate that the benefit that can be obtained from optimized window functions depends on the overlap between object spectrum and the Noise Power Spectrum, and thus on the sensitivity direction. We also find that sensitivity in z-direction yields a noise texture that is unsuitable for CT.

***Index Terms*—X-ray, phase-contrast, sensitivity direction, denoising**

I. Introduction

Recently, several measurement principles for X-ray phase contrast haven been proposed. Most notable of these are the Talbot-Lau interferometer [1], diffraction-enhanced systems [2] and coded apertures [3]. These systems share a common trait: they can only obtain differential phase-contrast contrast projection images along one sensitivity direction.

When performing CT acquisitions, these systems are typically operated such that the sensitivity direction is tangential to the CT trajectory, and thus radial to the rotation axis when rotating. For the Talbot-Lau interferometer (coded apertures) this means that the grating bars (the apertures) are parallel to the rotation axis. The noise behavior of this configuration has been studied extensively in [4], [5], [6].

In principle, the sensitivity axis can be chosen arbitrarily by rotating the phase-sensitive components of the system along the optical axis. For example, it has been shown that direction-dependent dark-field CT [7], [8] reconstruction can benefit from having the sensitivity direction in z-direction [9], i.e. parallel to the rotation axis. For a fan-beam-like geometry, z-sensitivity has the further advantage that the gratings (apertures) do not have to be bent to match the fan angle.

It is also conceivable to acquire two perpendicular directional derivatives. For geometries that can be approximated well using parallel beams, this can be realized relatively easily by using diagonal gratings (apertures) and has shown to yield reduced reconstruction noise when compared to the standard radial sensitivity approach [10].

In the this paper, we investigate the Noise Power Spectrum of a differential CT system depending on its sensitivity direction. We ignore the system-specific phase sensitivity and noise behavior to obtain a system-neutral analysis for CT reconstruction of differential projections. Specifically, we consider three configurations: the standard approach of radial sensitivity, sensitivity in z-direction and sensitivity in both directions (at half dose for each direction).

Additionally, we use the analytical Noise Power Spectrum and Wiener filtering to define noise-suppressing window functions for these configuration, as each shows a vastly different noise texture. To our knowledge, this is the first study of the noise behavior of non-standard sensitivity configuration and also the first paper to propose practicable window functions for differential CT.

II. Methods

In the following sections, we will derive the Noise Power Spectrum of differential CT and use this information to derive noise-suppressing window functions.

A. Noise Power Spectrum

We follow the simplified model of a parallel beam reconstruction with uniform projection Noise Power Spectrum and multiple slices with voxel and pixel size a as in [4]. In this case the total radial Noise Power Spectrum $\mathrm{NPS}_{\mathrm{tot}}$ is given by

$$\mathrm{NPS}_{\mathrm{tot}}(\rho_{\mathrm{r}}, \rho_{\mathrm{z}}) = f^2_{\mathrm{RamLak}} \cdot f_{\mathrm{invradon}} \cdot f^2_{\mathrm{interpol}} \cdot f^2_{\mathrm{integration}} \ . \tag{1}$$

Here, ρ_{r} denotes the radial frequency and ρ_{z} denotes the frequency in z-direction, i.e. across slices. For the RamLak filter we have $f_{\mathrm{RamLak}} = |\rho_{\mathrm{r}}| \cdot \mathrm{rect}(\rho_{\mathrm{r}}/2a)$, for Radon inversion we have $f_{\mathrm{invradon}} = 1/|\rho_{\mathrm{r}}|$ and for linear interpolation onto a grid of voxels with size a we have $f_{\mathrm{interpol}} = \mathrm{sinc}(\pi a \rho_{\mathrm{r}})^2 = [\sin(\pi a \rho_{\mathrm{r}})/(\pi a \rho_{\mathrm{r}})]^2$. This yields

$$\mathrm{NPS}_{\mathrm{tot}}(\rho_{\mathrm{r}}, \rho_{\mathrm{z}}) = |\rho_{\mathrm{r}}| \cdot \mathrm{rect}(\rho_{\mathrm{r}}/(2a)) \cdot \mathrm{sinc}(\pi a \rho_{\mathrm{r}})^4 \cdot f^2_{\mathrm{integration}} \ . \tag{2}$$

The frequency response $f^2_{\mathrm{integration}}$ for integrating the differential projections depends on the sensitivity direction. For the standard approach of radial sensitivity we have for a $[-1; 1]$ backward discretization of the derivative operator [4]

$$f^{\mathrm{rad}}_{\mathrm{integration}} = a/[2\sin(\pi a \rho_{\mathrm{r}})] \ . \tag{3}$$

All authors are with the the Pattern Recognition Lab, Department of Computer Science, Friedrich-Alexander-University Erlangen-Nuremberg. Contact: sebastian.kaeppler@fau.de
www5.cs.fau.de/%7Ekaeppler

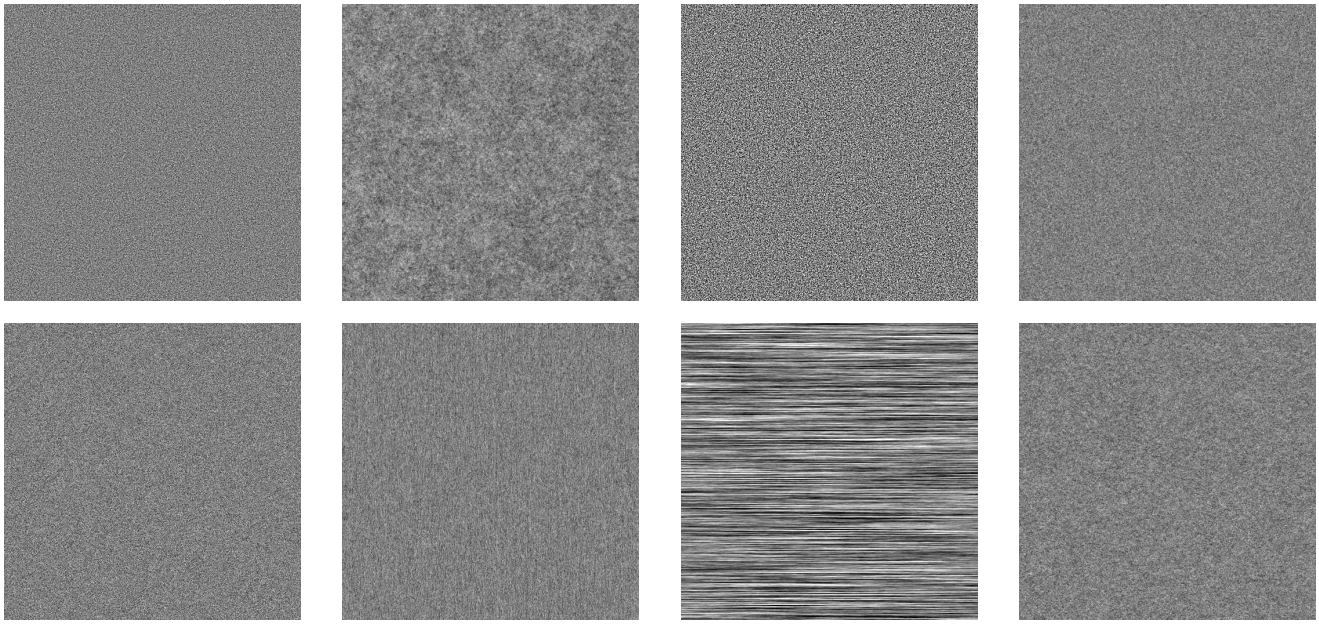

Fig. 1. Sample CT noise realizations displayed in arbitrary units, created as described in Section III. Top row: X-Y plane. Bottom row: X-Z plane. a) Non-differential projections. b) Differential (radial). c) Differential (z-direction) d) Differential (both directions). The linear scale is identical all images, except for the noise obtained for differential (z-direction), which was downscaled by a factor of five.

For sensitivity in z-direction we simply have to change the integration direction

$$f^{\mathrm{z}}_{\mathrm{integration}} = a/[2\sin(\pi a \rho_{\mathrm{z}})] \ . \tag{4}$$

Note that both integration steps assume that the object is non-truncated along the integration direction. Thus, having the sensitivity direction in z-direction requires not only a non-truncated object in radial direction (due to the inverse Radon transform) but also in z-direction (due to the integration across slices).

The frequency response of 2-D integration can be calculated by considering its closed form solution in Fourier domain, yielding

$$f^{\mathrm{2D}}_{\mathrm{integration}} = \sqrt{2}a/[2\sin(\pi a \rho_{\mathrm{r}}) + 2\sin(\pi a \rho_{\mathrm{z}})] \ . \tag{5}$$

Here, the prefactor $\sqrt{2}$ accounts for having only half of the dose for determining the image information for each direction. The non-truncation requirements of 2-D integration are relaxed compared to 1-D integration, here only one known pixel has to be outside of the object.

Each of the integration factors lead to the amplification of low frequency noise. For radial sensitivity $\mathrm{NPS}^{\mathrm{rad}}_{\mathrm{tot}} \rightarrow \infty$ for $\rho_{\mathrm{r}} \rightarrow 0$, although the frequency response of the ramp filter combined with the inverse Radon transform partially compensate the low-frequency noise induced by integration.

This is not the case for integration in z-direction, where $\mathrm{NPS}^{\mathrm{z}}_{\mathrm{tot}} \rightarrow \infty$ for $\rho_{\mathrm{z}} \rightarrow 0$. Here, ramp filtering acts as a high-pass in radial direction, while integration acts as a low-pass in z-direction, suggesting a noise pattern with a high autocorrelation in z-direction and negative autocorrelation in radial direction.

For 2-D integration $\mathrm{NPS}^{\mathrm{2D}}_{\mathrm{tot}} \rightarrow \infty$ only for $\rho_{\mathrm{r}}, \rho_{\mathrm{r}} \rightarrow 0$, indicating autocorrelated noise in both directions.

The quadratic scaling of the Noise Power Spectrum by the pixel size a is identical for all sensitivity directions and can thus be ignored when comparing the relative performance of sensitivity directions.

Sample CT noise realizations obtained by reconstructing the same amount of projection noise are shown in Fig. 1. The noise texture is in accordance with the noise autocorrelation behavior given by the Noise Power Spectrum. The approach with sensitivity in z-direction suffers from strong noise amplification due to integration being not aligned with ramp filtering.

B. Noise-Suppressing Windows

In the following, we will use Wiener Filtering to derive noise-suppressing window functions for differential CT. Note that in contrast to a conventional window function, our window not only operates in radial direction, but also in z-direction. Wiener filtering can be realized by applying window function $\mathbf{W}$ in Fourier domain. The frequency-dependent window function is given by the (also frequency-dependent) signal-to-noise ratio:

$$\mathbf{W} = \frac{1}{1 + \frac{1}{\mathrm{SNR}}} \ . \tag{6}$$

For CT, the signal-to-noise ratio depends on the object to be reconstructed and the noise. Both are unknown quantities, however the noise can be estimated using the analytical model of the Noise Power Spectrum (Eqn. 2). We thus require only an estimate of the Power Spectrum of the object, denoted as $\hat{\mathbf{O}}$, to estimate the SNR as $\hat{\mathbf{S}}$:

$$\hat{\mathbf{S}}(\rho_{\mathrm{r}}, \rho_{\mathrm{z}}) = \frac{\hat{\mathbf{O}}(\rho_{\mathrm{r}}, \rho_{\mathrm{z}})}{\mathrm{NPS}_{\mathrm{tot}}(\rho_{\mathrm{r}}, \rho_{\mathrm{z}})} \ . \tag{7}$$

This step allows to define the noise-suppressing window function independent on the noise behavior of the system.

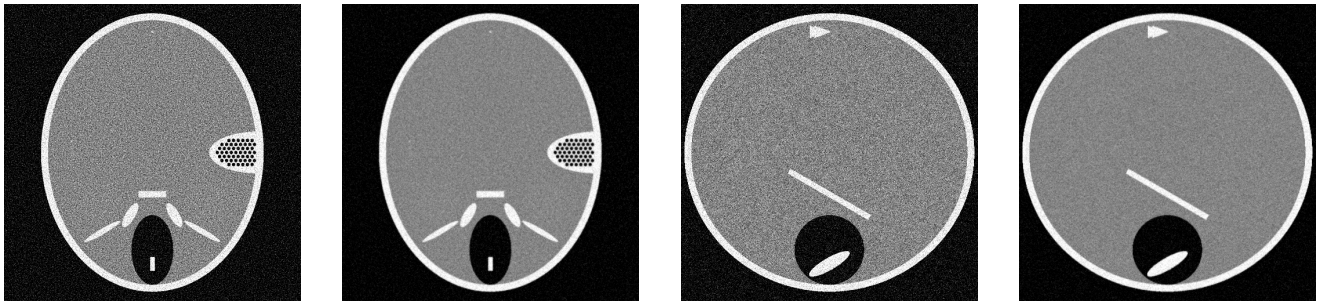

non-differential reconstruction, PSNR noisy: 11.7dB, PSNR denoised: 20.2dB (+8.5dB)

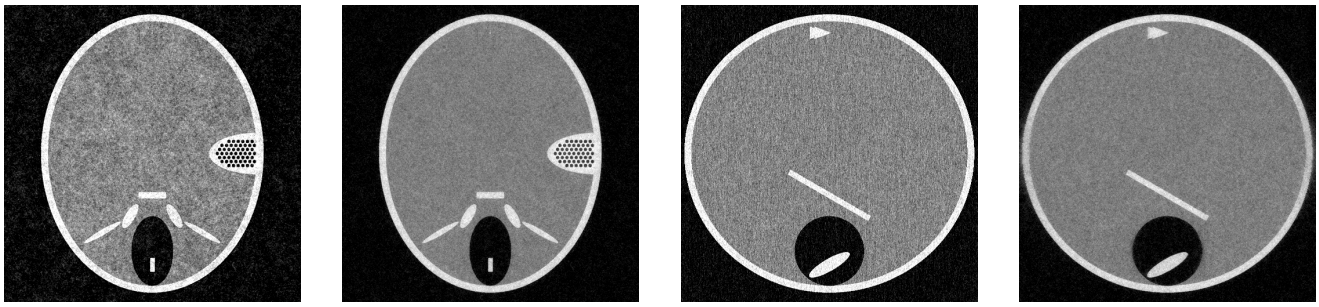

radial-differential reconstruction, PSNR noisy: 14.3dB, PSNR denoised: 18.0dB (+3.7dB)

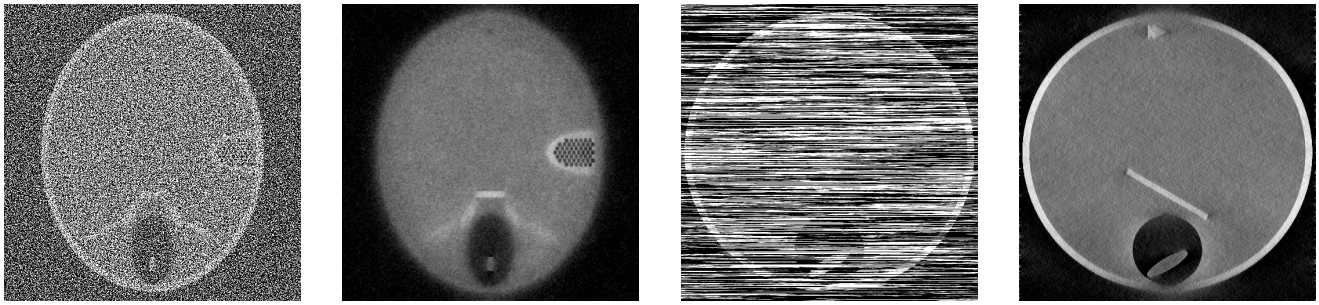

z-differential reconstruction, PSNR noisy: -7.4dB, PSNR denoised: 12.4dB (+19.0dB)

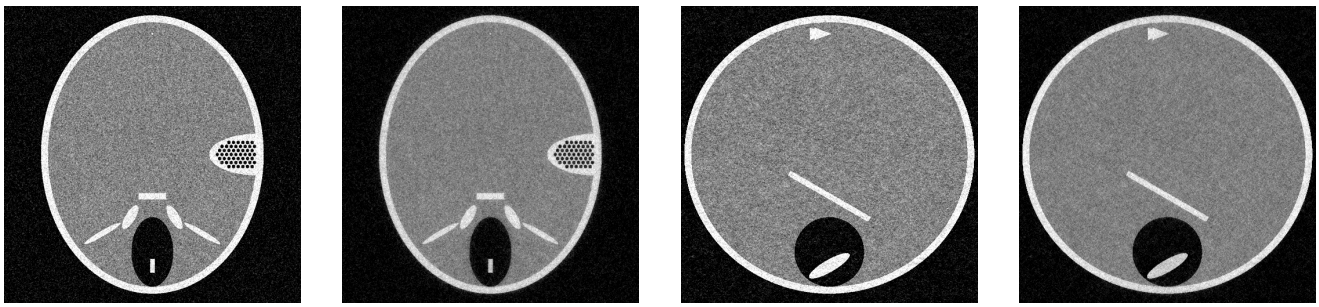

bi-differential reconstruction, PSNR noisy: 14.5dB, PSNR denoised: 17.2dB (+2.7dB)

a) b) c) d)

Fig. 2. Reconstruction results of applying the proposed Wiener window to modified version of the head phantom. a) central X-Y plane, noisy. b) central X-Y plane, denoised. c) central X-Z plane, noisy. d) central X-Z plane, denoised. The same intensity window has been applied to all images.

Note that by choosing an appropriate $\hat{\mathbf{O}}$, the tradeoff between reconstruction fidelity and noise can be attuned to objects of different contrast, shape, or size, given that the object is radially symmetric.

Due to the interchangeability of filtering and backprojection, the window function can also be applied to projections. This results in negligible computational demand for applying the window, as it involves replacing multiple 1-D Fourier transforms (for ramp filtering) with a single 2-D Fourier transform (for ramp filtering combined with the window function).

Note that for differential CT our approach of using a 2-D window function is more powerful than the conventional approach of using a radial window function combined with increasing the slice thickness, because the implicit frequency response of this approach is linearly separable in ρ_{r} and ρ_{z}, which is not optimal for the Noise Power Spectrum encountered in differential CT.

III. Experiments & Results

Before evaluating the proposed window function, we simulated Noise Power Spectra for all configurations and compared them with their analytic representations. They were in good agreement but are omitted in this paper due to space constraints.

For evaluating the proposed window function, we performed reconstruction of a modified version of the FORBILD head phantom onto a 512^3 grid with voxel size $0.5\mathrm{cm}^3$. Reconstruction parameters were selected to match our assumption of a parallel beam geometry, rectangular apodization, and linear interpolation. The angular increment was 0.5° to avoid angular undersampling. Projection images were of size 730×512 pixels with a pixel size identical to the voxel size. Projections were corrupted with additive white Gaussian noise. Reconstruction was performed once without and with the proposed window function.

Defining the window function requires knowledge of the Noise Power Spectrum and the Object Power Spectrum. For the Noise Power Spectrum, we used the analytic definition. The Object Power Spectrum needs to estimated. To this end, we assumed a spherically symmetric Power Spectrum which decays exponentially towards high frequencies. We model this power spectrum as:

$$\hat{\mathbf{O}}(\rho_\mathrm{r}, \rho_\mathrm{z}) = a \cdot x^b, \;\; x = \sqrt{\rho_\mathrm{r}^2 + \rho_\mathrm{z}^2} \;\; . \tag{8}$$

The model parameters a and b are estimated from the head phantom.[1]

Results of the evaluation with the peak signal-to-noise ratio (PSNR) are shown in Fig. 2. Applying the proposed window reduces reconstruction error for all approaches, and yields a more even residual noise texture.

The reconstruction obtained with z-sensitivity benefits most from denoising, due to the high amount of noise. Still, it suffers from a poor signal-to-noise ratio which renders the resulting images unusable.

The second most benefit can be observed in the non-differential reconstruction. We attribute this to the low overlap between Noise Power Spectrum and Object Power Spectrum. Here, our window shows the well-known tradeoff between resolution and noise in conventional CT.

The least benefit is observed for the reconstruction using two sensitivity axes. This can again be attributed to the overlap between Noise Power Spectrum and Object Power Spectrum. Here the overlap is high, since both spectra are strongest in the low frequencies.

Reconstruction using the standard approach with radial sensitivity yields a higher PSNR than the bi-directional approach after applying the window function, while its PSNR is lower when no window is used. We attribute this to the noise structure of this approach, which can relatively easily be attenuated by frequency adaptive smoothing in z-direction that is strong at low radial frequencies, and decays towards higher radial frequencies.

[1] Strictly speaking, this step violates the guidelines for proper parameter selection. However, we argue that if the shape of the Noise Power Spectrum is known, the Object Power Spectrum could also be estimated from the noisy reconstruction, yielding possibly even better performance.

IV. Conclusions

We have investigated the noise behavior of CT reconstruction from directional differential projections. Our experiments indicate that reconstructions from differential projections in z-direction suffer from high noise and are unusable in practice. This leads to a design conflict, as dark-field reconstruction can benefit from this configuration.

Reconstruction from two directional derivatives yields a more even noise texture than the standard radial approach. However, our experiments indicate that this can be mitigated by choosing an appropriate reconstruction window for the radial direction. We will investigate this finding in further studies.

Our investigation yields many directions for other future work. We plan to further investigate the shape of our window function for the different configurations, and to quantify the gain in reconstruction quality depending on the overlap between Object and Noise Power Spectrum. Additionally, we are interested in the implication of our findings for designing regularizers for iterative phase-contrast CT reconstruction.

References

[1] F. Pfeiffer, T. Weitkamp, O. Bunk, and C. David, "Phase Retrieval and Differential Phase-contrast Imaging with Low-brilliance X-ray Sources," *Nature Physics*, vol. 2, no. 4, pp. 258–261, Apr. 2006.

[2] C. Parham, Z. Zhong, D. Connor, L. Chapman, and E. Pisano, "Design and Implementation of a Compact Low-Dose Diffraction Enhanced Medical Imaging System," *Academic Radiology*, vol. 16, no. 8, pp. 911–917, Aug. 2009.

[3] A. Olivo and R. Speller, "A coded-aperture technique allowing x-ray phase contrast imaging with conventional sources," *Applied Physics Letters*, vol. 91, no. 7, pp. 074106, 2007.

[4] R. Raupach and T. Flohr, "Analytical Evaluation of the Signal and Noise Propagation in X-ray Differential Phase-Contrast Computed Tomography," *Physics in Medicine and Biology*, vol. 56, no. 7, pp. 2219–2244, Apr. 2011.

[5] C. Hagen, P. Diemoz, and A. Olivo, "On the relative performance of edge illumination x-ray phase-contrast ct and conventional, attenuation-based ct," *Medical Physics*, vol. 44, no. 5, pp. 1876–1885, 2017.

[6] K. Li, N. Bevins, J. Zambelli, and G.-H. Chen, "Fundamental relationship between the noise properties of grating-based differential phase contrast ct and absorption ct: Theoretical framework using a cascaded system model and experimental validation," *Medical Physics*, vol. 40, no. 2, 2013.

[7] A. Malecki, G. Potdevin, T. Biernath, E. Eggl, K. Willer, T. Lasser, J. Maisenbacher, J. Gibmeier, A. Wanner, and F. Pfeiffer, "X-ray tensor Tomography," *Europhysics Letters*, vol. 105, no. 3, pp. 38002, 2014.

[8] F. Bayer, S. Hu, A. Maier, T. Weber, G. Anton, T. Michel, and C. Riess, "Reconstruction of scalar and vectorial components in X-ray dark-field tomography," *Proceedings of the National Academy of Sciences of the United States of America*, vol. 111, no. 35, pp. 12699–12704, Sept. 2014.

[9] F. Schaff, F. Prade, Y. Sharma, M. Bech, and F. Pfeiffer, "Non-iterative directional dark-field tomography," *Scientific Reports*, vol. 7, 2017.

[10] S. Rutishauser, T. Donath, C. David, F. Pfeiffer, F. Marone, P. Modregger, and M. Stampanoni, "A tilted grating interferometer for full vector field differential x-ray phase contrast tomography," *Optics Express*, vol. 19, no. 25, pp. 24890–24896, 2011.